

Supplementary Information

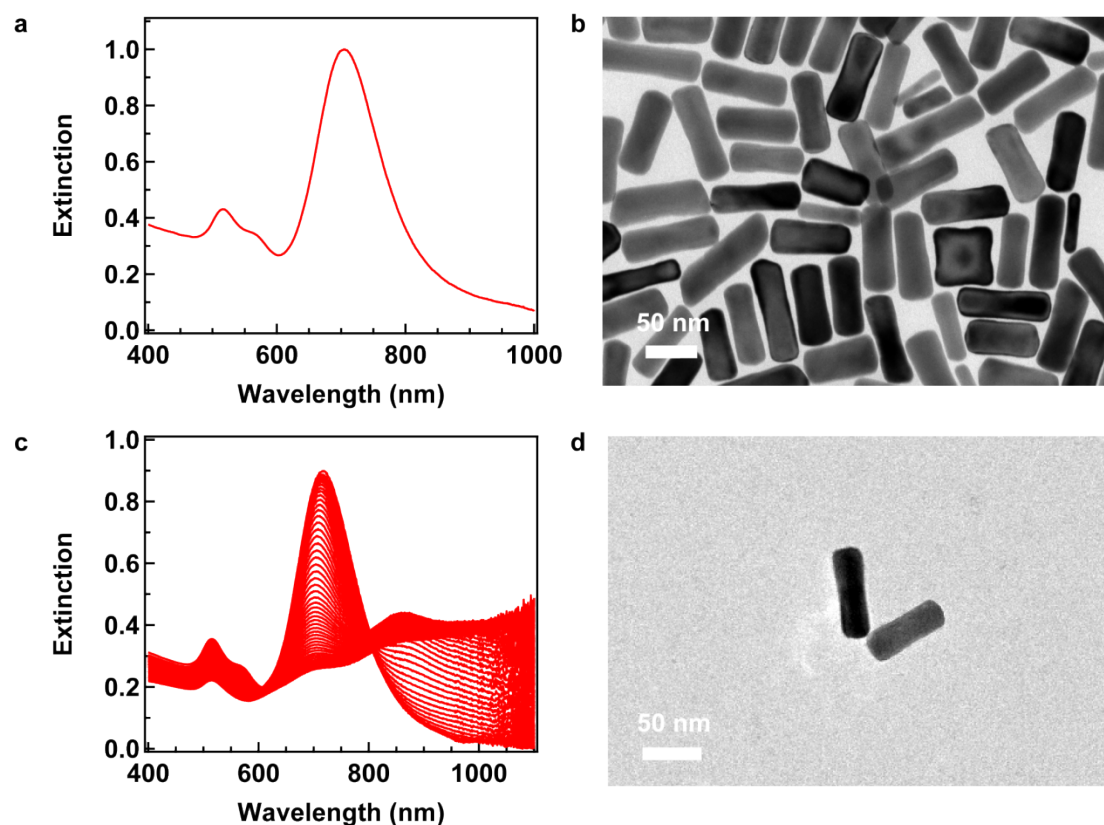


Figure S1. Preparation and CYS-assisted assembly of gold nanorods. (a) Extinction spectra of as-synthesized gold nanorods in solution. As-synthesized gold nanorods dispersed in 0.1 M CTAB solution show an ensemble LSPR wavelength at 704 nm. (b) The TEM image of the as-synthesized gold nanorods. The average diameter, length, and aspect ratio of the gold nanorods are 24 ± 2 nm, 69 ± 5 nm, and 2.9 ± 0.3 , respectively. (c) Time-dependent extinction spectra of gold nanorods acquired during the CYS-assisted assembly. The assembly of gold nanorods was monitored and recorded every 5 min. (d) The TEM image of a gold dimer.

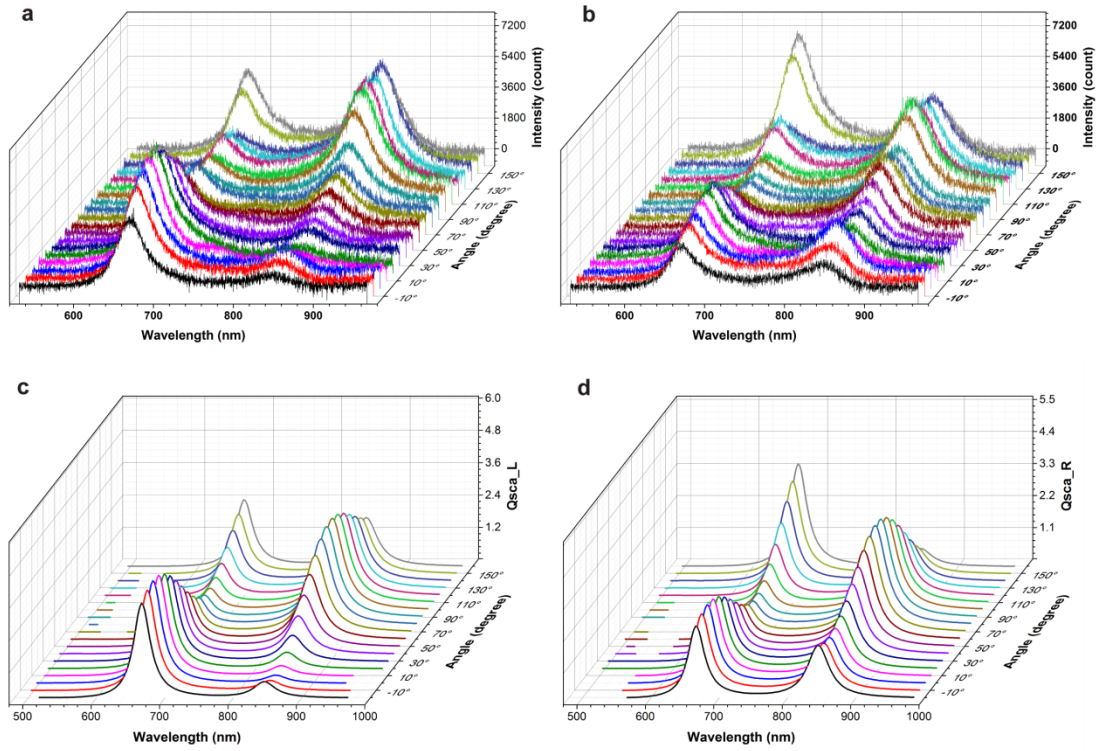


Figure S2. Scattering spectra of a dimer with $\beta = 80^\circ$ measured (up) and calculated (bottom) at various ϕ under the excitation of incident light with LCP (left) and RCP (right), respectively. The spectra were measured by rotating the sample stage clockwise at a step of 10° . The incident angle is 60° .

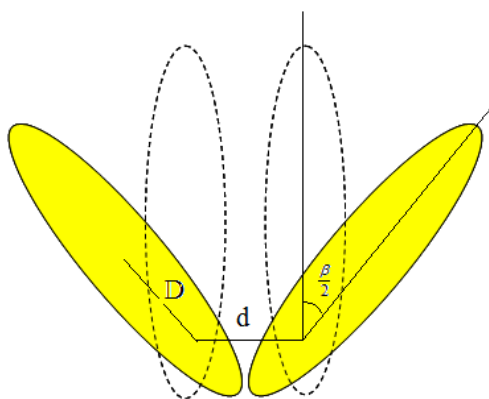


Figure S3. Schematic of the geometry used in CDA calculation. The gold nanorod dimer is modeled as two identical prolate ellipsoids surrounded by a homogeneous medium. β is the angle between the long axes of the two ellipsoids. d is indicated as the distance between the rotation points of the two ellipsoids. $a = 3.65b$, $D = 1.46b$, and $d = 2.2b$, where a and b are major and minor axis radii of the ellipsoid, respectively.

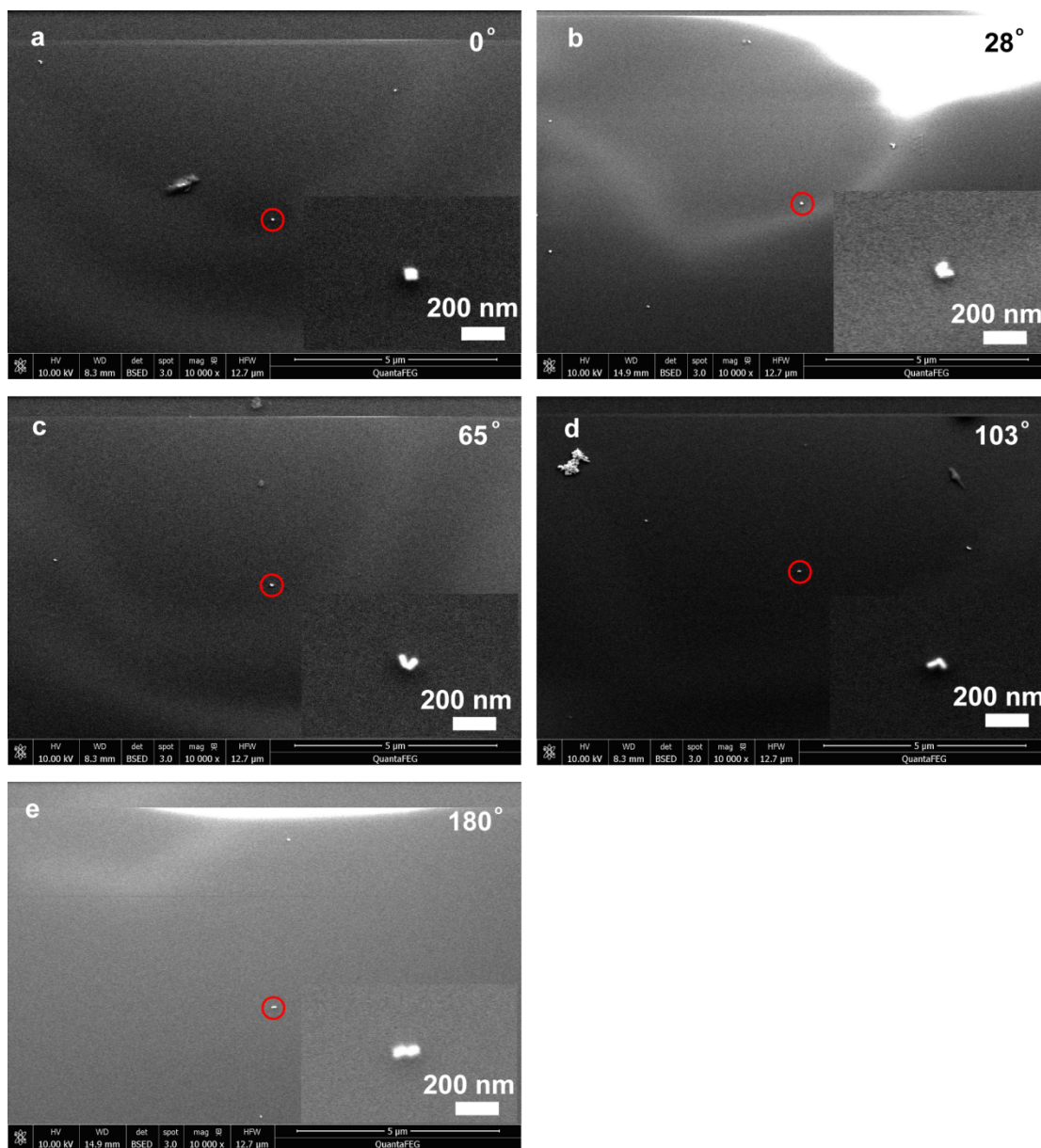


Figure S4. (a-e) SEM images of gold nanorod dimers with $\beta = 0^\circ$, 28° , 65° , 103° , and 180° , respectively. Insets show zoomed-in images for the dimers highlighted by circles. White stripes in the images are from the charging effect during the scanning of the electron beam.

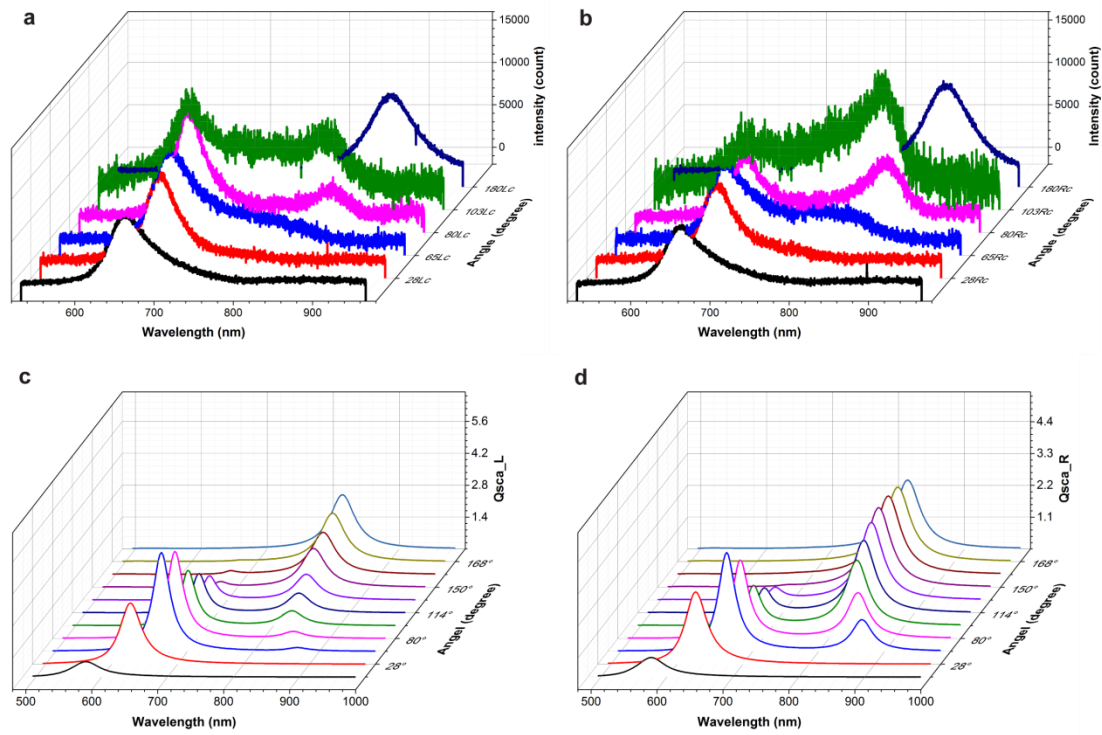


Figure S5. (a) Measured scattering spectra of gold nanorod dimers with $\beta = 0^\circ$, 28° , 65° , 80° , 103° , and 180° under the excitation of incident light with LCP. (b) Those for RCP. (c) Calculated spectra for $\beta = 0^\circ$, 28° , 65° , 80° , 103° , 114° , 126° , 150° , 156° , 168° , and 180° under the excitation of incident light with LCP. (d) Those for RCP.

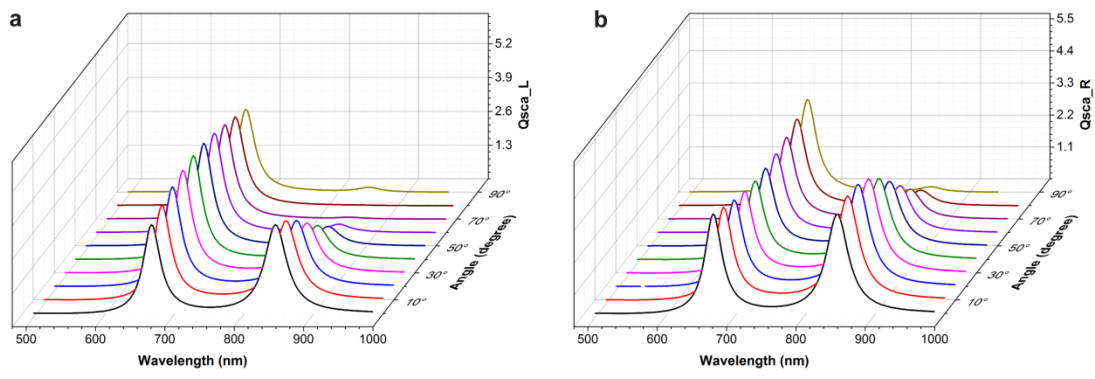


Figure S6. (a) Calculated scattering spectra of a dimer with $\beta = 80^\circ$ under the excitation of incident light with LCP at various incident angles. (b) Those for RCP.

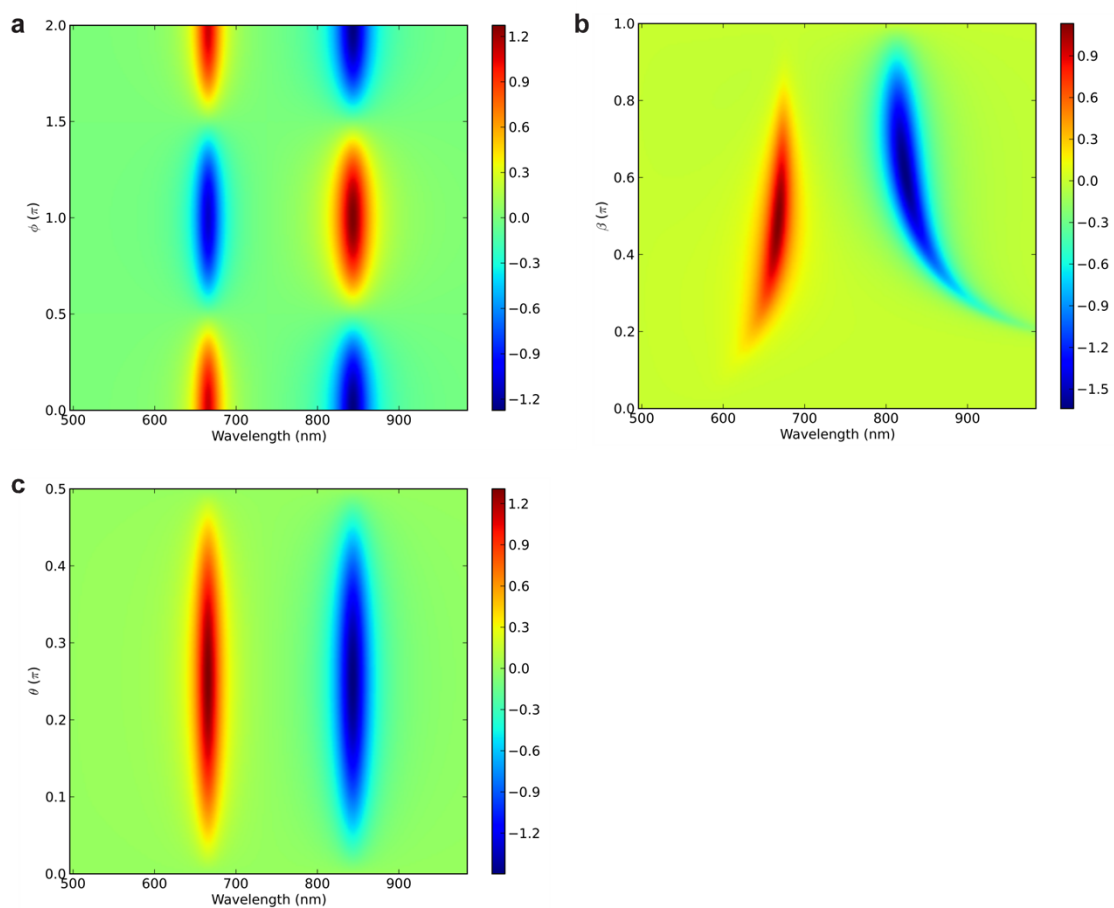


Figure S7. (a) Calculated 2D profile representing the scattering CD spectra for an arrangement with $\beta = 80^\circ$ and $\theta = 60^\circ$ at varying ϕ . (b) That for $\theta = 60^\circ$ and $\phi = 0^\circ$ at varying β . (c) That for $\beta = 80^\circ$ and $\phi = 0^\circ$ at varying θ .

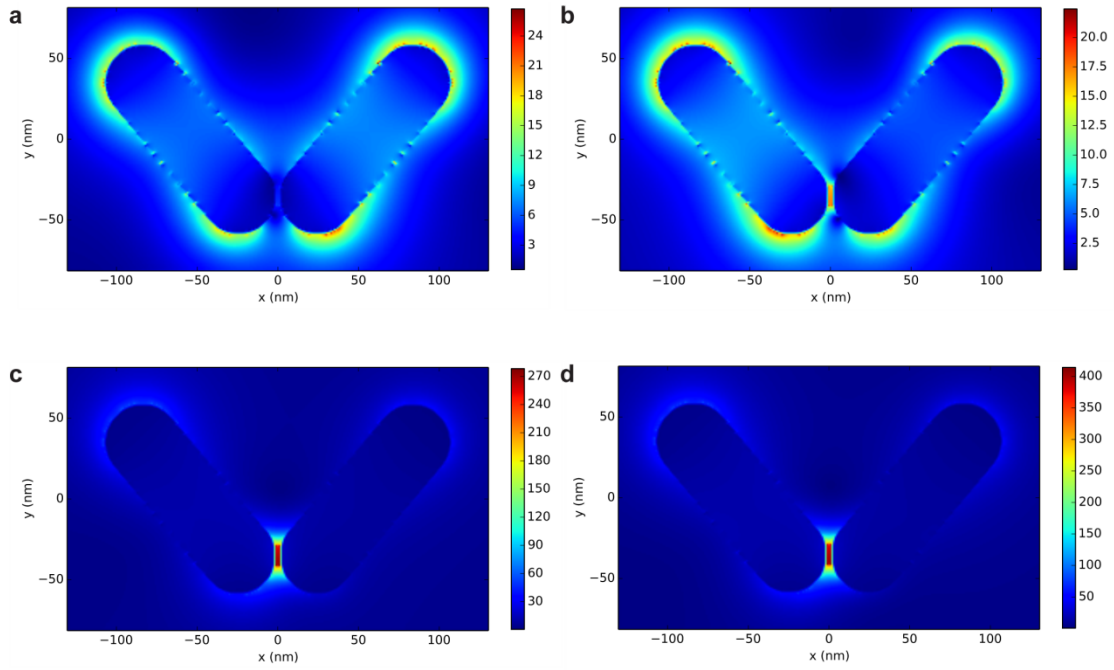


Figure S8. (a) FDTD-calculated E-field enhancement profile ($|E|/|E_0|$) for the gold nanorod dimer with $\beta = 80^\circ$ excited by an incident light with LCP at 1.87 eV (anti-bonding mode). The incident angle is 60° . The diameter and length of the gold nanorod are 23 nm and 69 nm respectively. The gap distance is 1 nm. (b) That for RCP. (c) That for LCP at 1.47 eV (bonding mode). (d) That for RCP at 1.47 eV (bonding mode).

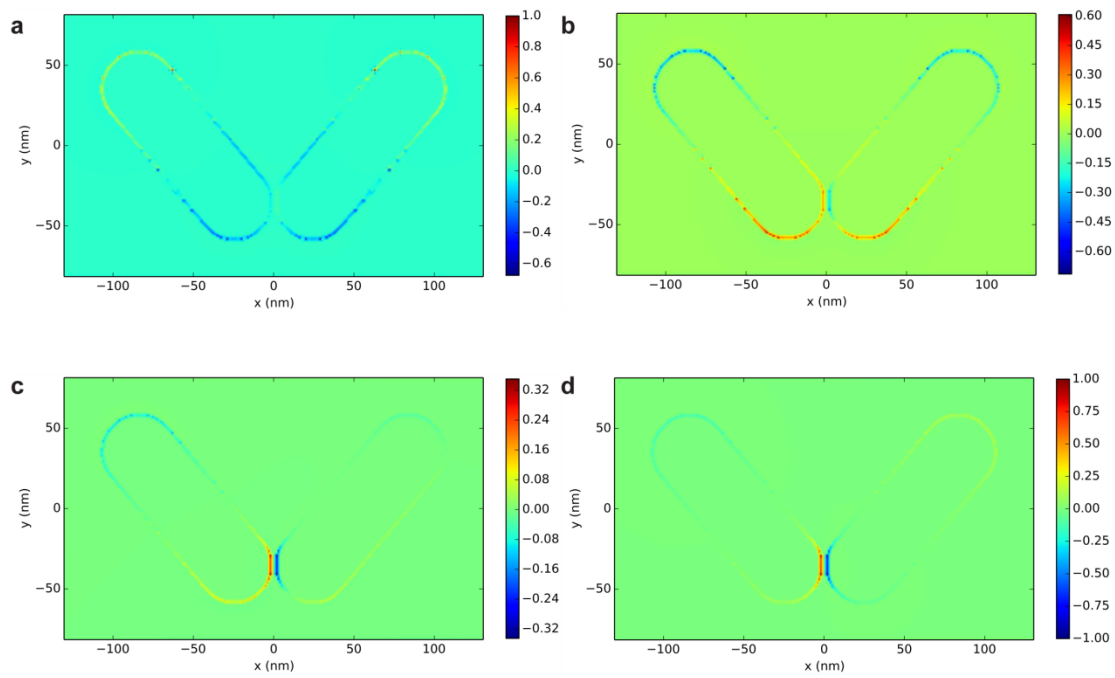


Figure S9. (a) Normalized electron charge distribution profile of the dimer excited by the incident light with LCP at 1.87 eV (anti-bonding mode). (b) That for RCP at 1.87 eV (anti-bonding mode). The profile is normalized according to the maximum values in (a). (c) That for LCP 1.47 eV (bonding mode). The profile is normalized according to the maximum values in (d). (d) That for RCP at 1.47 eV (bonding mode).

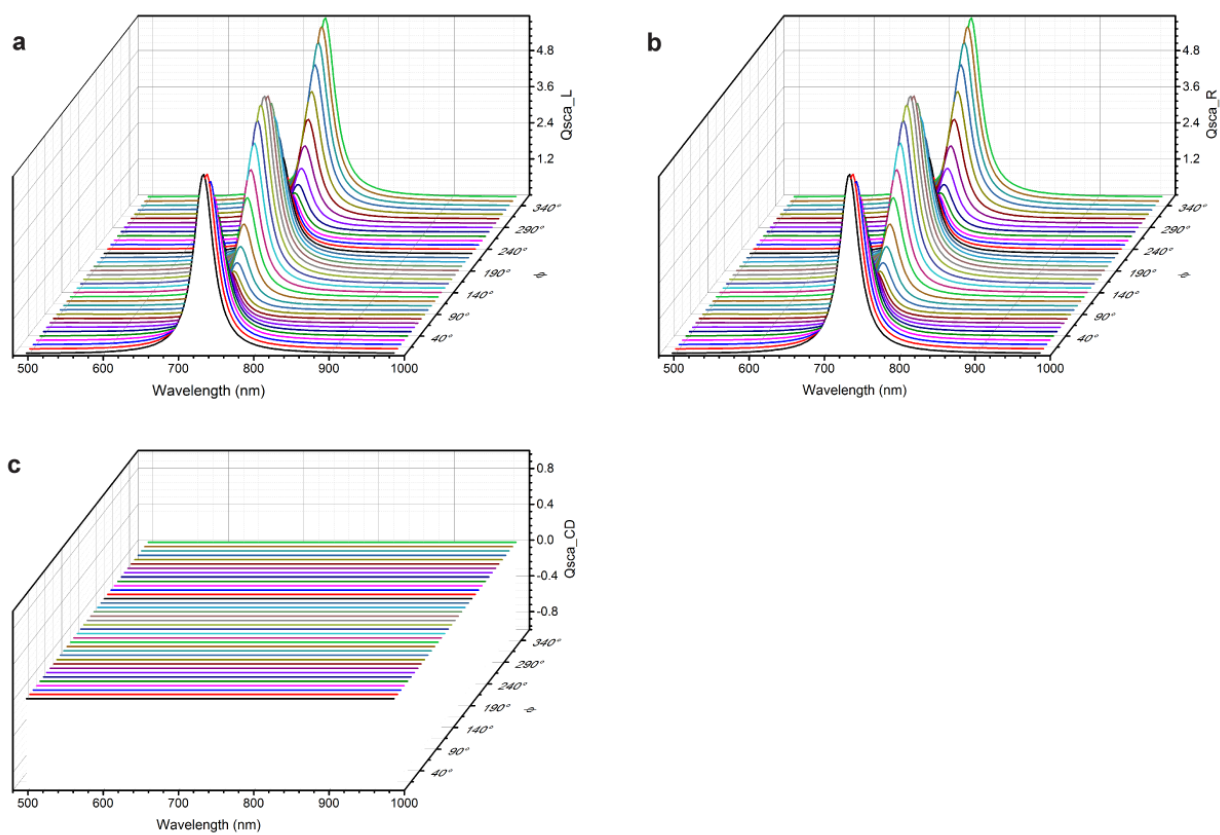


Figure S10. (a) Calculated scattering spectra of a single gold nanorod under the excitation of incident light with LCP at various azimuthal angles. (b) Those for RCP. (c) Its differential scattering spectra (LCP-RCP).

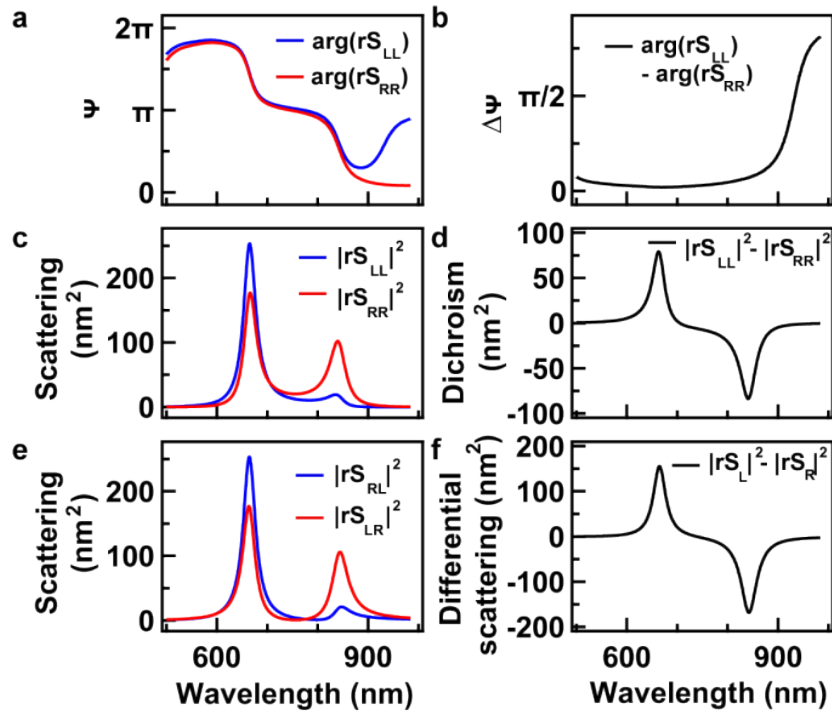


Figure S11. Mueller matrix elements for the scattering of circular polarized waves. (a) Dispersions of phase delay of LCP and RCP waves. (b) Difference of the phase delay. (c) Diagonal elements of the Mueller matrix for the LCP and RCP waves as a function of wavelength. (d) Circular dichroism Δ as a function of wavelength. (e) Those for off-diagonal elements of the Mueller matrix. (f) Difference of the total scattering intensity for LCP and RCP waves in corresponding to the measured differential scattering. Z-direction (direction to the microscope) scattering waves were considered in the calculations.

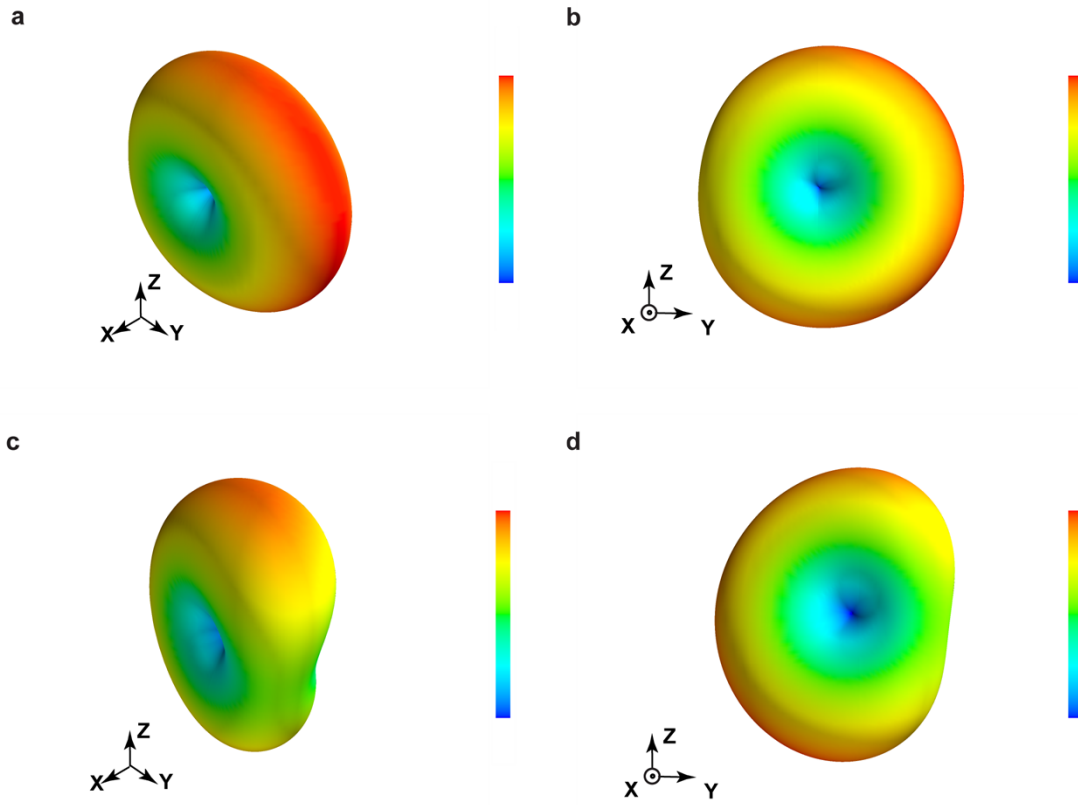


Figure S12. (a) Normalized far field scattering profile of the dimer excited by the incident light with LCP at 1.7 eV. (b) In the view along x-axis for (a). (c) That for RCP at 1.7 eV. (d) In the view along x-axis for (c).

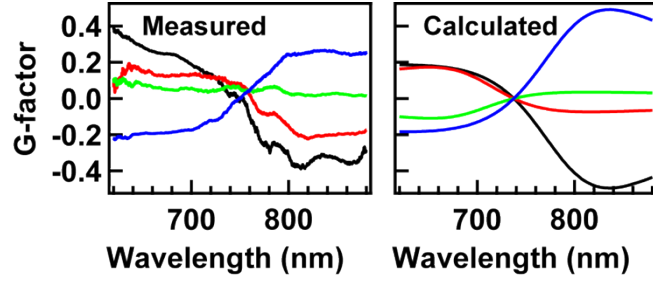


Figure S13. Comparison between measured and calculated g-factor plotted as a function of wavelength. The arrangement with $\beta = 80^\circ$ and $\theta = 60^\circ$ is measured and calculated at various $\phi = -20^\circ$ (black), 70° (red), 100° (green), and 160° (blue). The measured spectra were smoothed for better presentation. Here g-factor is evaluated according to

$$g = 2 \left(|rS_{LL}|^2 - |rS_{RR}|^2 \right) / \left(|rS_L|^2 + |rS_R|^2 \right).$$